EBioMedicine 65 (2021) 103255

Contents lists available at ScienceDirect

EBioMedicine

journal homepage: www.elsevier.com/locate/ebiom

Research paper

Camostat mesylate inhibits SARS-CoV-2 activation by TMPRSS2-related proteases and its metabolite GBPA exerts antiviral activity

Markus Hoffmann[a,b,*], Heike Hofmann-Winkler[a], Joan C. Smith[c,d], Nadine Krüger[a], Prerna Arora[a,b], Lambert K. Sørensen[e], Ole S. Søgaard[f,g], Jørgen Bo Hasselstrøm[e], Michael Winkler[a], Tim Hempel[h,i], Lluís Raich[h], Simon Olsson[h,j], Olga Danov[k], Danny Jonigk[k,l], Takashi Yamazoe[m], Katsura Yamatsuta[m], Hirotaka Mizuno[m], Stephan Ludwig[n,o], Frank Noé[h,i,p], Mads Kjolby[q,r,#], Armin Braun[k,#], Jason M. Sheltzer[d,#], Stefan Pöhlmann[a,b,*]

[a] *Infection Biology Unit, German Primate Center – Leibniz Institute for Primate Research, 37077 Göttingen, Germany*
[b] *Faculty of Biology and Psychology, University Göttingen, 37073 Göttingen, Germany*
[c] *Google, Inc., New York City, NY 10011, USA*
[d] *Cold Spring Harbor Laboratory, Cold Spring Harbor, NY 11724, USA*
[e] *Department of Forensic Medicine, Aarhus University, 8200 Aarhus, Denmark*
[f] *Department of Clinical Medicine, Aarhus University, 8200 Aarhus, Denmark*
[g] *Department of Infectious Diseases, Aarhus University Hospital, 8200 Aarhus, Denmark*
[h] *Freie Universität Berlin, Department of Mathematics and Computer Science, Berlin, Germany*
[i] *Freie Universität Berlin, Department of Physics, Berlin, Germany*
[j] *Chalmers University of Technology, Department of Computer Science and Engineering, Göteborg, Sweden*
[k] *Fraunhofer Institute for Toxicology and Experimental Medicine ITEM, Biomedical Research in Endstage and Obstructive Lung Disease Hannover (BREATH), Member of the German Center for Lung Research (DZL), Member of Fraunhofer International Consortium for Anti-Infective Research (iCAIR), Nikolai-Fuchs-Strasse 1, 30625 Hannover, Germany*
[l] *Institute of Pathology, Hannover Medical School, Biomedical Research in Endstage and Obstructive Lung Disease Hannover (BREATH), Hannover, Germany*
[m] *Discovery Technology Research Laboratories, Ono Pharmaceutical Co., Ltd., Osaka 618-8585, Japan*
[n] *Institute of Virology (IVM), Westfälische Wilhelms-Universität, 48149 Münster, Germany*
[o] *Cluster of Excellence "Cells in Motion", Westfälische Wilhelms-Universität, 48149 Münster, Germany*
[p] *Rice University, Department of Chemistry, Houston, TX, USA*
[q] *Danish Diabetes Academy and DANDRITE, Department of Biomedicine, Aarhus University, 8000 Aarhus, Denmark*
[r] *Department of Clinical Pharmacology, Aarhus University Hospital, 8200 Aarhus, Denmark*

ARTICLE INFO

Article History:
Received 20 August 2020
Revised 28 January 2021
Accepted 8 February 2021
Available online 4 March 2021

Keywords:
SARS-CoV-2
Camostat
TMPRSS2
GBPA
FOY-251

ABSTRACT

Background: Antivirals are needed to combat the COVID-19 pandemic, which is caused by SARS-CoV-2. The clinically-proven protease inhibitor Camostat mesylate inhibits SARS-CoV-2 infection by blocking the virus-activating host cell protease TMPRSS2. However, antiviral activity of Camostat mesylate metabolites and potential viral resistance have not been analyzed. Moreover, antiviral activity of Camostat mesylate in human lung tissue remains to be demonstrated.

Methods: We used recombinant TMPRSS2, reporter particles bearing the spike protein of SARS-CoV-2 or authentic SARS-CoV-2 to assess inhibition of TMPRSS2 and viral entry, respectively, by Camostat mesylate and its metabolite GBPA.

Findings: We show that several TMPRSS2-related proteases activate SARS-CoV-2 and that two, TMPRSS11D and TMPRSS13, are robustly expressed in the upper respiratory tract. However, entry mediated by these proteases was blocked by Camostat mesylate. The Camostat metabolite GBPA inhibited recombinant TMPRSS2 with reduced efficiency as compared to Camostat mesylate. In contrast, both inhibitors exhibited similar antiviral activity and this correlated with the rapid conversion of Camostat mesylate into GBPA in the presence of serum. Finally, Camostat mesylate and GBPA blocked SARS-CoV-2 spread in human lung tissue ex vivo and the related protease inhibitor Nafamostat mesylate exerted augmented antiviral activity.

Interpretation: Our results suggest that SARS-CoV-2 can use TMPRSS2 and closely related proteases for spread in the upper respiratory tract and that spread in the human lung can be blocked by Camostat mesylate and its metabolite GBPA.

* Corresponding author.
E-mail addresses: mhoffmann@dpz.eu (M. Hoffmann), spoehlmann@dpz.eu (S. Pöhlmann).
# Contributed equally.

https://doi.org/10.1016/j.ebiom.2021.103255

Funding: NIH, Damon Runyon Foundation, ACS, NYCT, DFG, EU, Berlin Mathematics center MATH+, BMBF, Lower Saxony, Lundbeck Foundation, Novo Nordisk Foundation.

Research in context

Evidence before this study

Antivirals are urgently needed to combat the SARS-CoV-2/COVID-19 pandemic. The SARS-CoV-2 activating host cell protease TMPRSS2 has been identified as an attractive target for antiviral intervention. Cleavage of the viral spike protein (S) by TMPRSS2 is essential for viral entry into lung cells and TMPRSS2 expression is dispensable for normal development and homeostasis in mice, indicating that TMPRSS2 inhibitors will block viral spread without eliciting major unwanted side effects. Indeed, a clinically-proven inhibitor of TMPRSS2, Camostat mesylate, was shown to block SARS-CoV-2 infection of primary human lung cells and was found to inhibit SARS-CoV spread and pathogenesis in mice. Thus, Camostat mesylate, which has a favorable safety profile, might be suitable for prevention and treatment of COVID-19 and related viral diseases, since SARS-CoV, MERS-CoV and several influenza A viruses depend on TMPRSS2 for spread and pathogenesis. However, it has been unknown whether SARS-CoV-2 can use TMPRSS2-related proteases for host cell entry and whether usage of these enzymes renders entry Camostat mesylate resistant. Moreover, it was unknown whether the major Camostat mesylate metabolite GBPA, which is rapidly generated in humans, exerts antiviral activity.

Added value of this study

The present study demonstrates that SARS-CoV-2 can employ TMPRSS2-related enzymes for cell entry and provides evidence that these enzymes may support viral spread in the upper respiratory tract. However, usage of TMPRSS2-related enzymes did not render viral entry Camostat mesylate resistant. Moreover, our results show that the Camostat mesylate metabolite GBPA blocks TMPRSS2 activity, although with reduced efficiency as compared to the parental compound, and we provide structural insights into how Camostat mesylate and GBPA block TMPRSS2. Finally, we demonstrate that GBPA is rapidly generated in cell culture and, in keeping with this finding, demonstrate that Camostat mesylate and GBPA exert similar antiviral activity.

Implications of all of the available evidence

All evidence available at present indicates that Camostat mesylate will suppress SARS-CoV-2 infection by blocking TMPRSS2 and related enzymes that can activate the viral S protein. Metabolization of Camostat mesylate will be compatible with antiviral activity, since the standard dose of Camostat mesylate (200 mg) results in a peak concentration of 0.25 μM in plasma, and likely also lung, which is above the EC_{50} measured for the Camostat mesylate metabolite GBPA, 0.178 μM. In fact, recent evidence suggests that GBPA blocks TMPRSS2 by covalently binding to the enzyme, which in conjunction with the slow GBPA metabolization, suggests that a single dose of Camostat mesylate might exert prolonged antiviral activity.

1. Introduction

The outbreak of the novel coronavirus severe acute respiratory syndrome coronavirus 2 (SARS-CoV-2) in the city of Wuhan, China, in the winter of 2019 and its subsequent pandemic spread has resulted in more than 65 million cases of coronavirus disease 2019 and more than 1.4 million deaths [1]. Antivirals designed to combat SARS-CoV-2 are not available and repurposing of existing drugs developed against other diseases is considered the fastest option to close this gap [2]. Remdesivir, a drug generated to inhibit Ebola virus infection, has recently been shown to reduce the duration of hospitalization for COVID-19 [3]. However, the drug failed to reduce fatality significantly [3] and beneficial effects were not observed in a previous clinical trial [4], indicating that additional therapeutic options are needed.

We previously showed that the SARS-CoV-2 spike protein (S) uses the host cell factors angiotensin-converting enzyme 2 (ACE2) and transmembrane protease serine 2 (TMPRSS2) for entry into target cells [5]. TMPRSS2 is a cellular type II transmembrane serine protease (TTSP) expressed in human respiratory epithelium that cleaves and thereby activates the viral S protein. Activation is essential for viral infectivity and we found that the protease inhibitor Camostat mesylate, which is known to block TMPRSS2 activity [6], inhibits SARS-CoV-2 infection of lung cells [5]. Camostat mesylate has been approved for treatment of pancreatitis in Japan [7–9] and it is currently being investigated as a treatment of COVID-19 in several clinical trials in Denmark, Israel and USA (NCT04321096, NCT04353284, NCT04355052, NCT04374019).

The activity of TMPRSS2 is essential for SARS-CoV and MERS-CoV lung infection and disease development [10,11]. Whether TMPRSS2-independent pathways for S protein activation exist and contribute to viral spread outside the lung is not fully understood. The S proteins of SARS-CoV-2 and several other coronaviruses can be activated by the pH-dependent endosomal cysteine protease cathepsin L in certain cell lines [5,12–15]. However, this auxiliary S protein activation pathway is not operative in the lung, likely due to low cathepsin L expression [16]. Whether this pathway contributes to the recently reported extrapulmonary spread of SARS-CoV-2 is unknown [17]. Similarly, it is unclear whether TTSPs other than TMPRSS2 can promote extrapulmonary SARS-CoV-2 spread. Finally, Camostat mesylate is rapidly hydrolyzed into the active metabolite 4-(4-guanidinobenzoyloxy)phenylacetic acid (GBPA) in patients [18–20] but it is unknown to what extend GBPA inhibits TMPRSS2 activity.

Here, we identify TTSPs other than TMPRSS2 that can be used by SARS-CoV-2 for S protein activation and demonstrate that they are inhibited by Camostat mesylate. Moreover, we provide evidence that Camostat mesylate is rapidly converted into GBPA in cell culture and that GBPA inhibits SARS-CoV-2 entry with almost identical efficiency as compared to Camostat mesylate when cells are preincubated with these compounds.

2. Methods

2.1. Cell culture

BHK-21 (baby hamster kidney; ATCC no. CCL-10, RRID: CVCL_1915), Vero E6 (African green Monkey kidney; ATCC no. CRL-1586, RRID:CVCL_0574), Vero-TMPRSS2 (Vero cells that stably

express TMPRSS2; [5]) and HEK-293T (human embryonic kidney; DSMZ no. ACC 635, RRID:CVCL_0063)) cells were cultivated in Dulbecco's modified Eagle medium supplemented with 10% fetal bovine serum (FCS, Biochrom), 100 U/mL of penicillin and 0.1 mg/mL of streptomycin (PAN-Biotech). Vero-TMPRSS2 cells further received 1 μg/ml blasticidin (Invitrogen). Calu-3 cells (human lung adenocarcinoma, RRID:CVCL_0609) were cultivated in minimum essential medium (MEM) containing 10% FCS (Biochrom), 100 U/mL of penicillin and 0.1 mg/mL of streptomycin (PAN-Biotech), 1x non-essential amino acid solution (from 100x stock, PAA) and 1 mM sodium pyruvate (Thermo Fisher Scientific). Cell lines were incubated at 37 °C in a humidified atmosphere containing 5% CO_2. Transfection of 293T cells was performed by calcium-phosphate precipitation, while Lipofectamine LTX with Plus reagent (Thermo Fisher Scientific) was used for transfection of BHK-21 cells. Authentication of cell lines was performed by STR-typing, amplification and sequencing of a fragment of the cytochrome c oxidase gene, microscopical examination and/or according to their growth characteristics. Further, cell lines were routinely tested for contamination by mycoplasma.

2.2. Plasmids

We employed pCAGGS-based expression vectors for VSV-G, TMPRSS2, TMPRSS3, TMPRSS4, TMPRSS10, TMPRSS11A, TMPRSS11B, TMPRSS11D, TMPRSS11E, TMPRSS11F and TMPRSS13 that have either been previously described elsewhere or constructed based on existing expression vectors [21–26]. All proteases contained an N-terminal cMYC-epitope tag. Further, we used pCG1-based expression vectors for human ACE2 [27] and a SARS-2-S variant with a truncated cytoplasmic tail for improved pseudotype particle production (deletion of last 18 amino acid residues [28].

2.3. Preparation of Camostat mesylate and GBPA stocks

Camostat mesylate and GBPA were obtained from Ono pharmaceuticals Co., LTD. (Osaka/Japan) and reconstituted in DMSO to yield stock solutions of 100 mM. Stocks were stored at -20 °C, thawed immediately before the experiment and residual compound was discarded.

2.4. Mass spectrometric quantification of Camostat mesylate metabolization

Camostat mesylate was diluted to a concentration of ~15 μM in either water or MEM containing 10% FCS and incubated for 1 min (water and medium samples), 15 min, 30 min, 1 h, 2 h, 4 h, 8 h and 24 h (only medium samples) at 37 °C. Next, samples were snap-frozen and stored at -80 °C until Camostat mesylate, GBPA (4-(4-guanidinobenzoyloxy) phenylacetic acid) and GBA (4-guanidinobenzoic acid) levels were quantified by mass spectrometry. An ultra-high-performance liquid chromatography tandem mass spectrometry method using pneumatically assisted electrospray ionisation (UHPLC-ESI-MS/MS) was used for quantification of Camostat and GBPA in liquid samples. Calibrants based on blank sample were used for the construction of 8-point calibration curves. Calibrants were prepared with concentrations of 0.1, 1, 25, 50, 75, 100, 500 and 1000 μg/L of Camostat and GBPA. In addition, a blank sample (a processed matrix sample without any added analyte) and a blank sample spiked with SIL-IS were included to verify the absence of detectable concentrations of the analytes. The calibration curves were created by weighted (1/x) regression analysis of the SIL-IS normalised peak areas (analyte area/IS area).

2.5. Preparation of pseudotype particles

We employed a previously published protocol to generate vesicular stomatitis virus (VSV) pseudotype particles that is based on a replication-deficient VSV containing eGFP and firefly luciferase (FLuc) reporter genes, VSV*ΔG-FLuc (kindly provided by Gert Zimmer, Institute of Virology and Immunology IVI, Mittelhäusern/Switzerland) [5,29]. For this, HEK-293T cells were first transfected with expression vector for either SARS-2-S or VSV-G (or empty expression vector, control). At 24 h post transfection, cells were inoculated with VSV-G-transcomplemented VSV*ΔG-FLuc at a multiplicity of infection (MOI) of 3 and incubated for 1 h at 37 °C and 5% CO_2. Next, the inoculum was removed and cells were washed with PBS before fresh culture medium was added. In case of cells transfected with SARS-2-S-encoding vector or empty plasmid, the medium was spiked with anti-VSV-G antibody (supernatant of CRL-2700 cells, 1:1,000, RRID: CVCL_G654) in order to inactivate residual input virus containing VSV-G. At 16−18 h post inoculation, the culture supernatant was harvested and centrifuged (2,000 x g,|10 min) to remove cellular debris. Clarified supernatants containing pseudotype particles were aliquoted and stored at -80 °C until further use.

2.6. Preparation of TMPRSS2 recombinant protein and substrate

Human TMPRSS2 (Recombinant N-terminus 6xHis, aa106-492) (Cat # LS-G57269-20) protein was acquired from LifeSpan Biosciences. Peptide Boc-Gln-Ala-Arg-MCA for the enzyme substrate was acquired from Peptide Institute, Inc.

2.7. TMPRSS2 enzyme assay

All different concentrations of test compounds were dissolved in DMSO and diluted with assay buffer (50 mM Tris-HCl pH 8.0, 154 mM NaCl) to the final DMSO concentration of 1%. Compound solution and Boc-Gln-Ala-Arg-MCA (10 μM final concentration) were added into black 384-well black plates (Greiner Bio-One). Then, the enzyme reaction was started by adding recombinant TMPRSS2 to a final concentration of 2 μg/ml. Fluorescence intensity was recorded using the Envision plate reader (PerkinElmer; excitation: 380 nm, emission: 460 nm) in 2 min intervals over 60 min at room temperature (RT). The 50 % effective concentration (EC_{50}) value was calculated based on the increasing rate of fluorescence intensity.

2.8. Molecular dynamics simulations and Markov modeling

We used extensive 50 μs all-atom molecular dynamics (MD) simulations of TMPRSS2 in complex with GBPA starting from a homology model [30], in which drug binding and dissociation are sampled multiple times. We have re-evaluated the Markov model [31] presented by Hempel and colleagues [32] to compare the dominant metastable TMPRSS2 binding mode populations of GBPA (Fig. 5) to camostat. At the simulated drug concentration, the association constant of GBPA is found to have a maximum likelihood estimate of 60% compared to that of Camostat mesylate, which, following the kinetic model described by Hempel et al [32], results in a correspondingly lower inhibitory activity. Bootstrapping of trajectories under the constraint of comparable implied timescales yields a confidence interval of 51−100% (68% percentile).

2.9. Transduction experiments

The day before transduction, BHK-21 cells were transfected with an expression vector for ACE2 and either empty expression plasmid (control) or expression vector encoding TMPRSS2, TMPRSS3, TMPRSS4, TMPRSS10, TMPRSS11A, TMPRSS11B, TMPRSS11D, TMPRSS11E, TMPRSS11F or TMPRSS13. For this, the old culture medium was removed and 50 μl/well of fresh culture medium were added. Next, transfection mixtures were prepared. For one well 0.1 μg of ACE2-encoding vector and 0.02 μg of protease-encoding vector (or empty plasmid) were mixed with 0.2 μl of Plus reagent, 50

μl of Opti-MEM medium (Thermo Fisher Scientific) and 0.2 μl of Lipofectamine LTX reagent. The transfection mix was vortexed and incubated for 30 min at RT before it was added to the cells. At 6 h post transfection, the transfection medium was replaced by fresh culture medium and the cells were further incubated for ~18 h. Then, the cells were either pre-incubated for 2 h with inhibitor (50 mM ammonium chloride [Sigma-Aldrich], 100 μM Camostat mesylate or a combination of both; cell treated with DMSO served as controls) before transduction or directly inoculated with pseudotype particles bearing SARS-2-S. For transduction of Calu-3 cells, cells were pre-incubated for 2 h at 37 °C and 5% CO_2 with different concentrations (0.01, 0.1, 1, 10, 100 μM) of Camostat mesylate, FOY-251 or DMSO (control), before they were inoculated with pseudotype particles bearing SARS-2-S or VSV-G. At 16 h post inoculation, transduction efficiency was analyzed by measuring the activity of virus-encoded FLuc in cell lysates. For this, the cell culture medium was removed and cells were incubated for 30 min with 1x concentrated Cell Culture Lysis Reagent (Promega), before cell lysates were transferred into white, opaque-walled 96-well plates and luminescence was recorded (1 s/sample) using a Hidex Sense plate luminometer (Hidex) and a commercial substrate (Beetle-Juice, PJK).

2.10. Analysis of cell vitality

For the analysis of cell vitality of Calu-3 cells treated with Camostat mesylate or FOY-251 the CellTiter-Glo Luminescent Cell Viability Assay kit (Promega) was used. For this, Calu-3 cells were grown in 96-well plates to reach ~50% confluency, before they were incubated in the presence of different concentrations of Camostat mesylate or FOY-251 for 24 h. Cells treated with DMSO (solvent control) served as controls. Following incubation, 100 μl of CellTiter-Glo substrate were added per well and the samples were incubated for 30 min on a rocking platform. In addition, fresh culture medium (without cells) was also incubated with CellTiter-Glo substrate in order to define the assay background. Following incubation, the samples were transferred into white, opaque-walled 96-well plates and luminescence was recorded (200 m/sample) using a Hidex Sense plate luminometer (Hidex).

2.11. Infection of Calu-3 cells with authentic SARS-CoV-2

The SARS-CoV-2 isolate hCoV-19/Germany/FI1103201/2020 (GISAID accession ID: EPI-ISL_463008) was isolated at the Institute of Virology, Muenster, Germany, from a patient returning from the Southern Tyrolean ski areas and propagated in Vero-TMPRSS2 cells. Calu-3 cells were pre-incubated for 2 h with 2-fold concentrated Camostat mesylate or FOY-251 (2, 20 or 200 μM), or DMSO (control), before they were inoculated with SARS-CoV-2 at an MOI of 0.001 or 0.01. For this, the identical volume of virus-containing medium was added to the inhibitor-containing medium on the cells (resulting in 1-fold concentrated Camostat mesylate or FOY-251; 1, 10 or 100 μM). Following 1 h of incubation at 37 °C and 5% CO_2, the culture supernatant was removed and cells were washed two times with excess PBS before culture medium containing 1-fold concentrated inhibitor was added. Supernatants were harvested at 24 h post inoculation and subjected to plaque titration. For this, confluent Vero-TMPRSS2 cells were inoculated with 10-fold serial dilutions of supernatant and incubated for 1 h 37 °C and 5% CO_2. Thereafter, the inoculum was removed and cells were incubated with culture medium containing 1% (w/v) methyl cellulose. Plaques were counted at 48 h post infection and titers determined as plaque forming units per ml (pfu/ml).

2.12. SARS-CoV-2 infection of precision-cut lung slices

Precision-cut lung slices (PCLS) were prepared from lung tissue acquired from patients who underwent lobe resection due to lung cancer at the Hannover Medical School (MHH, Hannover, Germany). Only macroscopically disease-free parts of the lung were used for experiments. Human lung slices with peripheral airways were prepared as described before [33]. Briefly, a lung lobe was inflated with 2% agarose/DMEM/F12 solution. After the agarose polymerization, the lung lobe was cut into slabs and tissue cores of 8 mm in diameter were cut into 300 μm thin slices. PCLS were maintained in Ham's F12 medium supplemented with 0.1 mg/ml streptomycin, 10 U/ml penicillin, 0.05 mg/ml gentamicin and 0.01 mg/ml enrofloxacin. Prior to infection, PCLS were placed in 48-well plates and checked for ciliary activity by light microscopy. Only PCLS displaying a ciliary activity of 75% or higher were selected for the experiments. Next, PCLS were pre-incubated for 2 h at 37 °C and 5% CO_2 with Camostat mesylate, FOY-251 or Nafamostat mesylate (0.5 μM or 5 μM) or received medium containing DMSO (solvent control). Thereafter, the culture supernatant was removed and PCLS were infected for 1 h at 37 °C and 5% CO_2 with SARS-CoV-2 isolate hCoV-19/Germany/FI1103201/2020 (GISAID accession ID: EPI_ISL_463008)using an infectious dose of 4×10^5 pfu/ml (250 μl/well). Following infection, the inoculum was removed and PCLS were washed three times with PBS before 500 μl culture medium containing the respective inhibitor or DMSO was added. At 1 h (washing control) and 24 h (end point) post infection, 100 μl supernatant were collected and stored at -80 °C for virus titration.

Virus titration was performed on Vero E6 cells (grown 12-well plates), which were inoculated for 1 h at 37 °C and 5% CO_2 with 850 μl of serial dilutions of the collected supernatants. Subsequently, the inoculum was removed and cells were washed one time with PBS, before they were overlaid with 1% plaque agarose (Biozym)-containing Eagle's minimal essential medium without phenol red (Lonza) and further incubated. Plaques were counted at 72 h post infection and titers determined as pfu/ml.

2.13. Analysis of TTSP expression in transfected cells by immunoblot

HEK-293T cells were grown in 12-wellplates and transfected with expression vector coding for the respective TTSP (containing an N-terminal cMYC-epitope tag) or empty expression vector. At 16 h post-transfection, the culture medium was replenished and cells were further incubated for 24 h at 37 °C and 5% CO^2. Next, the culture medium was removed, 150 μl of 2x SDS lysis buffer (5% glycerin, 1% SDS, 2.5% ß-mercaptoethanol, 0.5% bromophenol blue, 0.5 mM EDTA, 0.5 M Tris; pH 6.8) were added per well and samples were incubated for 10 min before they were transferred into 1.5 ml reaction tubes and heated to 95 °C for 15 min. Subsequently, lysates were subjected to SDS-PAGE (using 12.5% polyacrylamide gels) before proteins were transferred onto nitrocellulose membrane (GE Healthcare) using the Mini-PROTEAN Tetra Cell system (Bio-Rad). Following blocking of the membranes in 5% milk solution (blotting-grade milk powder [Carl Roth] dissolved in PBS containing 0.05% Tween-20 [AppliChem]; PBS-T) for 1 h at RT, membranes were incubated over night at 4 °C in either anti-cMYC antibody (clone 9E10)-containing hybridoma cell supernatant (mouse, RRID:CVCL_G671; TTSP expression) or 5% milk containing anti-ß-actin antibody (mouse, 1:1,000, Sigma-Aldrich, RRID: AB_476744; loading control). Afterwards, the membranes were washed three times with PBS-T before they were incubated for 1 h at RT in 5% milk solution containing horseradish peroxidase-coupled anti-mouse antibody (1:2,000, Dianova, RRID: AB_10015289). Finally, membranes were washed three times with PBS-T, incubated with an in house-prepared developing solution (1 ml of solution A: 0.1 M Tris-HCl [pH 8.6], 250 μg/ml luminol sodium salt; 100 μl of solution B: 1 mg/ml para-hydroxycoumaric acid dissolved in dimethyl sulfoxide [DMSO]; 1.5 μl of 0.3% H_2O_2 solution) and imaged using the ChemoCam imager along with the ChemoStar Imager Software (version v.0.3.23; Intas Science Imaging Instruments GmbH).

2.14. Analysis of TTSP expression in human proximal and distal airways by single cell RNAseq

Bulk tissue expression data were obtained from the GTEx portal [34]. The main site of lung specimen collection for the GTEx project was the inferior segment of the left upper lobe, 1 cm below the pleural surface. Single-cell expression data from human lungs were obtained from GSE1229603. Only IPF and cryobiopsy lung explants were used in this analysis. Single-cell expression data from human airways was obtained from https://www.genomique.eu/cellbrowser/HCA/4. The single-cell data was analyzed as described in Smith et al [35]. In short, dimensionality reduction and clustering were performed on normalized expression data in python using Scanpy and the Multicore-TSNE package [36,37]. Low quality cells were filtered out by removing cells with fewer than 500 detected genes. Highly variable genes were computed using the Seurat approach in Scanpy, and then used to calculate the principle component analysis. T-SNE and Leiden clustering were calculated using nearest neighbors, with parameters as described in the associated code. Cell clusters were labeled manually by comparing the expression patterns of established marker genes with the lists of differentially-expressed genes produced by Scanpy [38–41]. The code used for performing these analyses is available at https://github.com/joan-smith/covid19-proteases/.

2.15. Statistical analyses

All statistical analyses were performed using GraphPad Prism (version 8.4.2, GraphPad Software, Inc.). Statistical significance of differences between two datasets was analyzed by paired, two-tailed student's t-test while one- and two-way analysis of variance (ANOVA) with Dunnett's posttest was used for comparison of multiple datasets (the exact method used is stated in the figure legends). Effects were considered statistically significant when *P* values were 0.05 or lower. For the calculation of the turnover time required for metabolization of 50% of Camostat mesylate ($T_{1/2}$) as well as the EC_{50} values, which indicate the inhibitor concentration leading to 50% reduction of transduction, non-linear fit regression models were used.

2.16. Ethics

Experiments with human lung tissue were approved by the Ethics Committee of the Hannover Medical School (MHH, Hannover, Germany) and are in compliance with The Code of Ethics of the World Medical Association (number 2701-2015). All patients or their next of kin gave written informed consent for the use of lung tissue for research.

2.17. Role of funders

T.Y., K.Y., and H.M. are employees of Ono Pharmaceutical Co. and performed research (T.Y., K.Y.) and analyzed data (H.M.). J.C.S. is an employee of Google, Inc., but this work was performed outside of her affiliation with Google and used no proprietary knowledge or materials from Google. Sources of third party or institutional funding had no role in the design of the study, data collection and analysis and manuscript writing.

3. Results

3.1. Identification of novel SARS-CoV-2 S protein activating proteases

The TTSP family comprises several enzymes which have previously been shown to activate surface glycoproteins of coronaviruses and other viruses, at least upon directed expression [22,24,26]. Therefore, we asked whether the S protein of SARS-CoV-2 (SARS-2-S) can employ TTSPs other than TMPRSS2 for its activation. For this, we first confirmed expression of the proteases by immunoblot using antigenically tagged proteins. All proteases were expressed, although at different levels, and for some more than one band was detected, likely reflecting precursor (zymogen) and mature forms of the proteases (Fig. 1a and Fig. S1). Next, we expressed different TTSPs along with the SARS-CoV-2 receptor, ACE2, in the otherwise non-susceptible cell line BHK-21, treated the cells with ammonium chloride, which blocks the cathepsin L-dependent, auxiliary activation pathway, and transduced the cells with previously described vesicular stomatitis virus (VSV)-based pseudotypes bearing SARS-2-S [5]. Ammonium chloride treatment strongly reduced SARS-2-S-driven transduction and transduction was rescued upon expression of

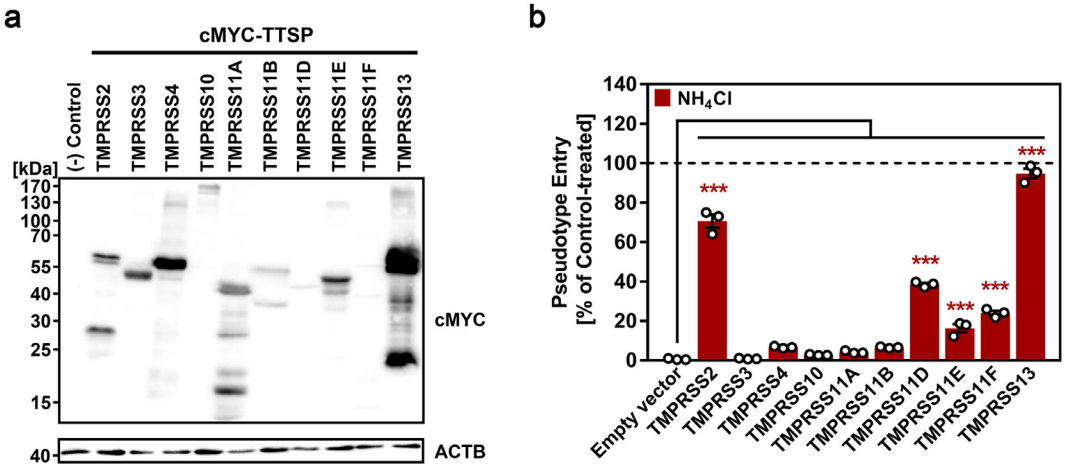

Fig. 1. Different type-II transmembrane serine proteases (TTSPs) can activate SARS-2-S in transfected cells. (**a**) The indicated TTSPs equipped with an N-terminal C-MYC antigenic tag were transiently expressed in 293T cells and expression analyzed by immunoblot with anti-C-MYC antibody. Detection of ß-actin (ACTB) served as loading control. Similar results were obtained in three biological replicates. (**b**) BHK-21 cells transiently expressing ACE2 and one of the indicated TTSPs (or empty vector) were pre-incubated with either 50 mM ammonium chloride or DMSO (control, indicated by dashed line) for 2 h, before they were inoculated with particles pseudotyped with SARS-2-S. At 16 h post inoculation, SARS-2-S-driven cell entry of viral pseudotypes was analyzed by measuring the activity of virus-encoded luciferase activity in cell lysates. Data were further normalized and entry efficiency in the absence of ammonium chloride was set as 100 % (indicated by dashed line). Shown are the average (mean) data obtained from three biological replicates, each performed with four technical replicates. Error bars indicate the standard error of the mean (SEM). Statistical significance of differences in entry efficiency in the presence of ammonium chloride was analyzed by two-way analysis of variance (ANOVA) with Dunnett's posttest (P values, from left to right: 0.0001; 0.9999; 0.0620; 0.9140; 0.4900; 0.0685; 0.0001; 0.0001; 0.0001; 0.0001).

TMPRSS2 (Fig. 1b), as expected. Notably, transduction was also efficiently rescued by expression of TMPRSS13 and, to a lesser degree, TMPRSS11D, TMPRSS11E and TMPRSS11F (Fig. 1b). Thus, SARS-2-S can use diverse TTSPs for S protein activation upon overexpression, with S protein activation by TMPRSS13 being particularly robust.

3.2. Several novel SARS-2-S activators are expressed in the airways and throat

In order to obtain insights into whether SARS-2-S activating TTSPs could contribute to viral spread in the infected host, we asked whether these enzymes are expressed in viral target cells. For this, we analyzed single-cell RNA-Seq datasets collected from human lungs [42] and airways [43]. As previously reported [35,44–48], ACE2 was expressed in the lung epithelial compartment, particularly including alveolar type 2 cells, secretory (goblet/club) cells, and ciliated cells (Fig. 2a and Fig. S2). TMPRSS2 and TMPRSS13 were similarly expressed across epithelial cells, although TMPRSS13 expression was generally less robust. In contrast, expression of TMPRSS11-family members was only rarely detected (Fig. 2a). We found that 53% of $ACE2^+$ cells in the lung co-express TMPRSS2, while 21% of $ACE2^+$ cells do not express TMPRSS2 but do express another TTSP capable of activating SARS-CoV-2 (Fig. S2). Within the airways, we observed ACE2 expression in secretory cells, ciliated cells, and suprabasal cells in both the nasal turbinate and the trachea (Fig. 2b). Interestingly, the expression pattern of the TTSPs in the airways was largely distinct: TMPRSS2 was primarily expressed in ciliated and secretory cells, TMPRSS11D was primarily expressed in basal cells, TMPRSS11E was primarily expressed in ionocytes, and TMPRSS13 was primarily expressed in nasal secretory cells (Fig. 2b). Within this dataset, 21% of $ACE2^+$ cells co-expressed TMPRSS2, while 24% of $ACE2^+$ cells co-expressed a different TTSP (Fig. S2). We note that in both the lungs and the airways, TTSP expression is largely restricted to the epithelial cell compartment, underscoring the fact that epithelial cells are the primary cell population targeted by SARS-CoV-2 (Fig. S3). In total, these results suggest that TMPRSS2 is the dominant SARS-CoV-2-activating protease in the lung, in keeping with findings made for SARS-CoV and MERS-CoV, while the virus may use other activating proteases for spread in the airways.

A recent study provided evidence for extrapulmonary replication of SARS-CoV-2 in liver, colon, heart, kidney and blood in some patients [17]. Therefore, we asked whether ACE2, TMPRSS2 and related SARS-2-S-activating proteases are expressed in these organs, using published resources [34,49]. Liver, colon, heart and kidney expressed robust levels of ACE2 (Fig. 2c). Similarly, TMPRSS2 expression in colon, liver and kidney was readily detectable, although expression levels were lower than those measured for lung (Fig. 2c). In contrast, little to no expression of TMPRSS11D, TMPRSS11E, TMPRSS11F and TMPRSS13 was detected in liver, colon, heart and kidney. Finally, TMPRSS13 was expressed in lung and blood cells and expression of TMPRSS11-family members was readily detectable in esophagus and salivary gland (Fig. 2c). Collectively, the TTSPs able to activate SARS-2-S were not expressed in appreciable levels in potential extrapulmonary targets of SARS-CoV-2. The only exceptions were TMPRS13 and TMPRSS11-family members that might contribute to SARS-CoV-2 infection of blood cells and to viral spread in the throat, respectively.

3.3. Newly identified SARS-2-S activators are Camostat mesylate sensitive

We next asked whether S protein activation by TTSP other than TMPRSS2 can be inhibited by Camostat mesylate. To address this question, we performed the rescue assay as described above but investigated whether rescue can be blocked by Camostat mesylate. In the absence of TTSP expression in target cells, ammonium chloride but not Camostat mesylate reduced SARS-2-S-driven entry and the combination of both substances resulted in similar inhibition as observed upon ammonium chloride treatment alone (Fig. 3). These results are in agreement with only the cathepsin L-dependent auxiliary pathway being operative in control BHK-21 cells, in agreement with our published results [5]. In TMPRSS2 transfected cells ammonium chloride did not efficiently block entry (Fig. 3), since under those conditions TMPRSS2 is available for S protein activation. Similarly, no entry inhibition was observed upon blockade of TMPRSS2 activity by Camostat mesylate (Fig. 3), since the cathepsin L-dependent activation pathway remained operative. Finally, the combination of ammonium chloride and Camostat mesylate blocked entry into these cells (Fig. 3), in keeping with both activation pathways (cathepsin L and TMPRSS2) not being available under these conditions. Importantly, a comparable inhibition pattern was observed for all TTSPs able to activate SARS-2-S (Fig. 3), demonstrating that Camostat mesylate will likely suppress SARS-CoV-2 activation by TMPRSS2 and TMPRSS2-related S protein activating serine proteases.

3.4. The Camostat mesylate metabolite GBPA shows reduced inhibition of recombinant TMPRSS2

Multiple studies show that Camostat mesylate is rapidly converted into its active metabolite, 4-(4-guanidinobenzoyloxy)phenylacetic acid (GBPA) in animals and humans, followed by further conversion of GBPA into the inactive metabolite 4-guanidinobenzoic acid (GBA) [18–20,50] (Fig. 6a). However, the capacity of GBPA to inhibit the enzymatic activity of TMPRSS2 has not been examined. To address this question, we compared inhibition of recombinant TMPRSS2 by Camostat mesylate, GBPA and GBA. For this, we used FOY-251, a methanesulfonate of GBPA, which is readily commercially available. We found that FOY-251 exerted a 10-fold reduced capacity to inhibit TMPRSS2 as compared to Camostat mesylate, although both compounds completely suppressed TMPRSS2 activity at 1 μM or higher (Fig. 4). In contrast, GBA was less active (Fig. 4). Thus, FOY-251 blocks TMPRSS2 activity but with reduced efficiency as compared to Camostat mesylate.

In order to obtain insights into the reduced inhibitory activity of FOY-251, we investigated TMPRSS2 inhibition by GBPA on the molecular level. For this, we used a combination of extensive all-atom molecular dynamics (MD) simulations and Markov modeling of the TMPRSS2-GBPA complex [32]. Guanidinobenzoate-containing drugs such as Camostat mesylate and GBPA inhibit TMPRSS2 by first forming a noncovalent precomplex which is then catalyzed to form a long-lived covalent complex that is the main source of inhibition [32]. However, the population of the short-lived precomplex directly relates to the inhibitory activity [32]. By computing the TMPRSS2-GBPA binding kinetics [32], we find that (i) the noncovalent TMPRSS2-GBPA complex is metastable, rendering it suitable to form a covalent inhibitory complex, and (ii) its population is 40% lower compared to Camostat at equal drug concentrations, consistent with the finding that FOY-251 is a viable but less potent inhibitor (Fig. 4). Structurally, we find that GBPA binds in the same manner as Camostat (Fig. 5, [32]). The main stabilizing interaction is its guanidinium group binding into TMPRSS2's S1 pocket, which is stabilized by a transient salt bridge with Asp-435. The GBPA ester group can interact with the catalytic Ser-441, making it prone for catalysis and formation of the catalytic complex. The slightly lower stability of the GBPA compared to the Camostat mesylate-TMPRSS2 complex is consistent with GBPA's shorter tail, which has less possibilities to interact with the hydrophobic patch on the TMPRSS2 binding site shown in Fig. 5, left panel.

3.5. Rapid conversion of Camostat mesylate to GBPA in cell culture

Although Camostat mesylate is rapidly metabolized in animals and humans, it is less clear whether conversion of Camostat mesylate

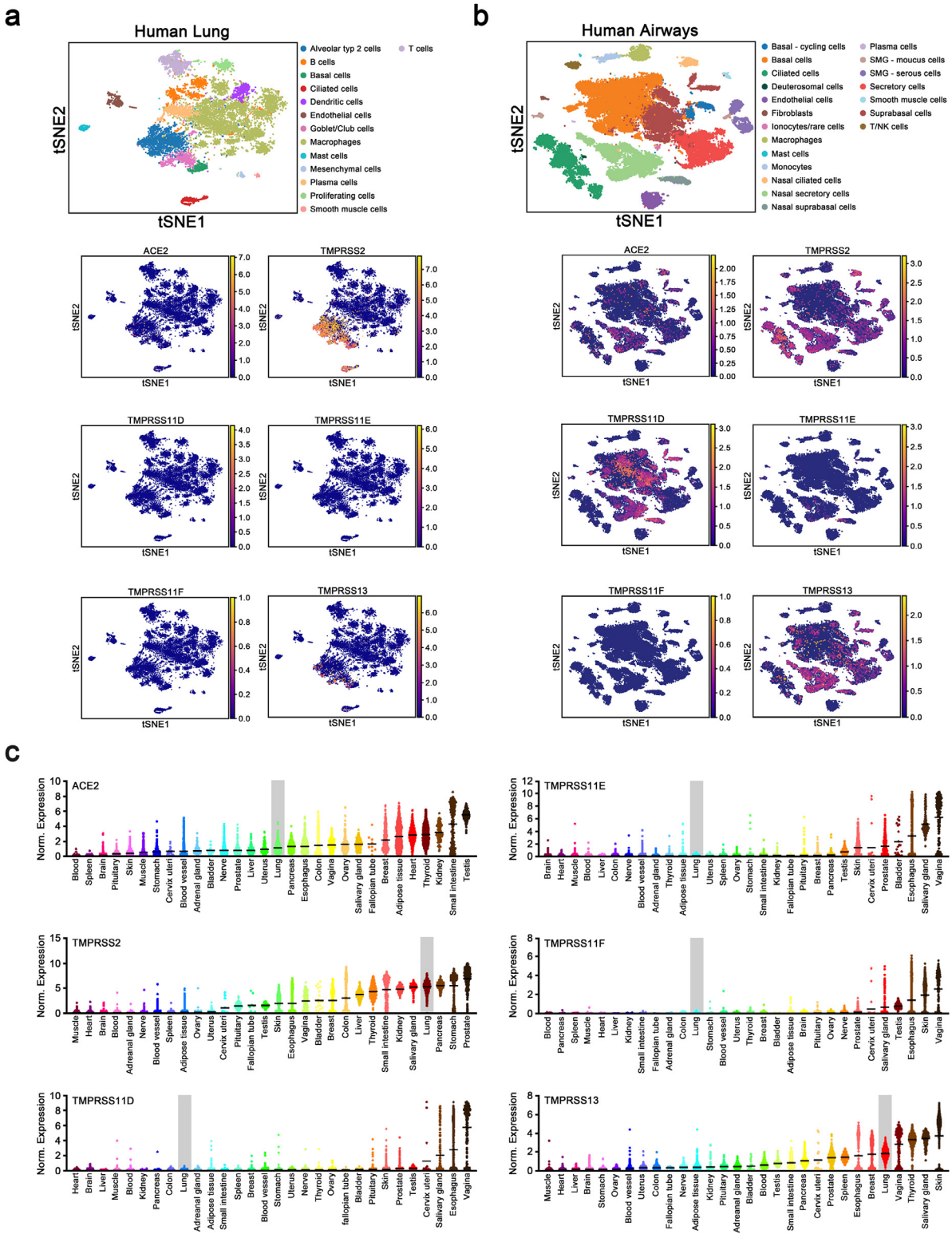

Fig. 2. SARS-2-S activating proteases are expressed in lung and blood. (**a**) T-SNE clustering of cells from the human lung [42]. Cells expressing the coronavirus receptor ACE2 are highlighted in the right panel. These panels are reproduced with permission from Smith et al. [35]. Cells expressing various S-activating proteases in the human lung are highlighted. (**b**) T-SNE clustering of cells from the human airway [43]. Cells expressing the coronavirus receptor ACE2 and the various S-activating proteases in the human airway are highlighted. (**c**) Log2-normalized expression data of the indicated genes across different human tissues from the GTEx consortium [34]. Certain panels are reprinted from "Cigarette Smoke Exposure and Inflammatory Signaling Increase the Expression of the SARS-CoV-2 Receptor ACE2 in the Respiratory Tract", Developmental Cell 53, Joan C. Smith, Erin L. Sausville, Vishruth Girish, Monet Lou Yuan, Anand Vasudevan, Kristen M. John, Jason M. Sheltzer, 514–529, Copyright (2020), with permission from Elsevier.

into GBPA also occurs in cell culture. We addressed this question by exposing Camostat mesylate to culture medium containing fetal calf serum (FCS), which is standardly used for cell culture, followed by mass spectrometric quantification of Camostat mesylate and GBPA levels. Camostat mesylate levels rapidly declined with a half-life of approximately 2 h and the compound being barely detectable after

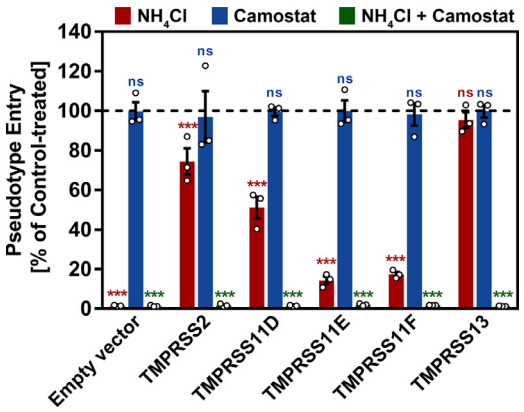

Fig. 3. Activation of SARS-2-S by TMPRSS2-related proteases can be suppressed by Camostat mesylate. The experiment was performed as described for Fig. 1 with the modifications that only TMPRSS2, TMPRSS11D, TMPRSS11E, TMPRSS11F and TMPRSS13 were investigated and target cells were pre-treated with either 50 mM ammonium chloride (red), 100 μM Camostat mesylate (blue) or a combination of both (green). DMSO-treated cells served as controls. At 16 h post inoculation with viral particles bearing SARS-2-S, pseudotype entry was analyzed by measuring virus-encoded luciferase activity in cell lysates. Data were further normalized and entry efficiency into control-treated cells was set as 100%. Shown are the average (mean) data obtained from three biological replicates, each performed with four technical replicates. Error bars indicate the SEM. Statistical significance of differences in entry efficiency in ammonium chloride-, Camostat mesylate- or ammonium chloride + Camostat mesylate-treated cells versus control-treated cells was analyzed by two-way ANOVA with Dunnett's posttest (*P* values, from left to right: NH_4Cl [0.0001; 0.0001; 0.0001; 0.0001; 0.0001; 0.7334]; Camostat [0.9999; 0.8995; 0.9969; 0.9999; 0.9731; 0.9999]; NH_4Cl/Camostat [0.0001; 0.0001; 0.0001; 0.0001; 0.0001; 0.0001]).

8 h (Fig. 6b). Conversely, the levels of the Camostat mesylate metabolite GBPA increased rapidly, with peak levels attained at 8 h, and then remained relatively stable (Fig. 6b). Finally, the rapid metabolization of Camostat mesylate into GBPA in the presence of serum was further confirmed by incubation of Camostat mesylate in either water or FCS-containing culture medium for 1 min followed by quantification of Camostat mesylate and GBPA levels. While GBPA levels were at background level when Camostat mesylate was incubated in water, ~5.4% of Camostat mesylate was metabolized into GBPA when incubated in FCS-containing culture medium (Fig. 6c). Thus, Camostat mesylate is rapidly converted into GBPA under standard cell culture conditions, but the conversion is slower than what is observed in humans [20].

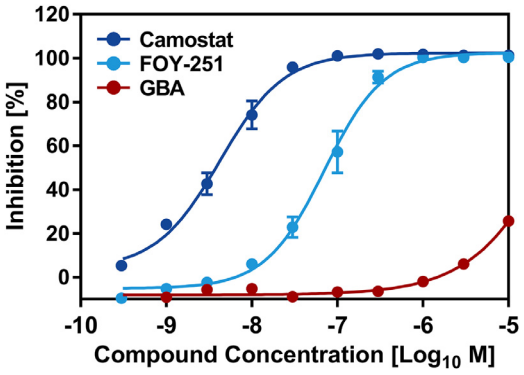

Fig. 4. Camostat mesylate and FOY-251 inhibit the activity of recombinant TMPRSS2. Incubation of recombinant TMPRSS2 with the Boc-Gln-Ala-Arg-MCA peptide substrate leads to the cleavage of the substrate and the release of the AMC(7-Amino-4-methylcoumarin) fluorophore, resulting in a fluorescent signal. Data were normalized against the fluorescence signals obtained in the absence of test compounds (Camostat mesylate, FOY-251, GBA). The concentration-response data for each test compound were plotted and modeled by a four-parameter logistic fit to determine the 50% effective concentration (EC_{50}) value. Inhibitory activity of Camostat mesylate (blue), FOY-251 (light blue) and GBA (red) against TMPRSS2 recombinant protein were visualized and curve fitting was performed using GraphPad Prism. The average of two biological replicates, each performed with four (Camostat mesylate and FOY-251) or two technical replicates (GBA) is shown. EC_{50} values were 4 nM (Camostat mesylate), 70 nM (FOY-251), >10 μM (GBA).

3.6. Camostat mesylate and FOY-251 inhibit SARS-CoV-2 infection with comparable efficiency

We finally compared the antiviral activity of Camostat mesylate and FOY-251, the methanesulfonate of GBPA, in cell culture. The reduced ability of FOY-251 to block the enzymatic activity of recombinant TMPRSS2 as compared to Camostat mesylate would suggest that the compound should also exert reduced antiviral activity. On the other hand, analysis of antiviral activity encompasses preincubation of target cells with Camostat mesylate for 2 h in the presence of FCS, which allows conversion of Camostat mesylate into GBPA, as demonstrated above. Indeed, titration experiments with VSV pseudotypes and Calu-3 lung cells as targets revealed that entry inhibition by FOY-251 was only slightly reduced as compared to Camostat mesylate, with EC_{50} values of 107 nM (Camostat mesylate) and 178 nM (FOY-251) (Fig. 7). Moreover, no marked differences in inhibition of infection of Calu-3 cells with authentic SARS-CoV-2 were observed (Fig. 8a). Finally, both Camostat mesylate and FOY-251, as well as another promising serine protease inhibitor for treatment of SARS-CoV-2 infections, Nafamostat mesylate, inhibited SARS-CoV-2 infection of human precision-cut-lung slices (PCLS) ex vivo, and again no major differences in inhibition efficiency were observed between Camostat mesylate and FOY-251 (Fig. 8B). Thus, under the conditions chosen Camostat mesylate and GBPA exerted roughly comparable antiviral activity, likely due to conversion of Camostat mesylate into GBPA.

4. Discussion

With the exception of Remdesivir, which reduces disease duration (3), and dexamethasone, which reduces mortality in intensive care unit (ICU) patients by targeting inflammation [51], there are currently no drugs against COVID-19 with efficacy proven in clinical trials. We previously reported that the protease inhibitor Camostat mesylate inhibits SARS-CoV-2 infection of cultured lung cells by blocking the virus-activating cellular protease TMPRSS2 [5]. Camostat mesylate has been approved for human use in Japan and may thus constitute a COVID-19 treatment option [52]. Here, we provide evidence that the virus can use TMPRSS2-related proteases for S protein activation and that these enzymes are also blocked by Camostat mesylate. Moreover, we demonstrate that the Camostat mesylate metabolite GBPA exhibits reduced ability to block enzymatic activity of purified, recombinant TMPRSS2 and is rapidly produced under cell culture conditions. The rapid conversion of Camostat mesylate into GBPA likely accounts for our finding that both compounds exerted similar antiviral activity.

Knock-out of TMPRSS2 in mice markedly reduces SARS-CoV and MERS-CoV infection [10] and disease development, and similar findings have been reported for influenza A viruses (IAV) [53–55], which also use TMPRSS2 for glycoprotein activation [56]. Thus, TMPRSS2 activity is essential for CoV and IAV infection of the lung. In contrast, several members of the TTSP family other than TMPRSS2 can activate CoV and IAV glycoproteins and support viral spread in cell culture, at least upon directed expression [24,26,56]. Whether these TTSPs play a role in viral spread in the host is incompletely understood. For IAV, infection by H3N2 viruses was found not to be fully TMPRSS2 dependent [53,57] and an auxiliary role of TMPRSS4 in spread and pathogenesis of H3N2 viruses has been reported [58,59]. Moreover, influenza B viruses can use a broad range of TTSPs in cell culture [59,60] and a prominent role of TMPRSS2 in viral spread in type II pneumocytes has been reported [61] but viral spread in mice is TMPRSS2 independent [59,62].

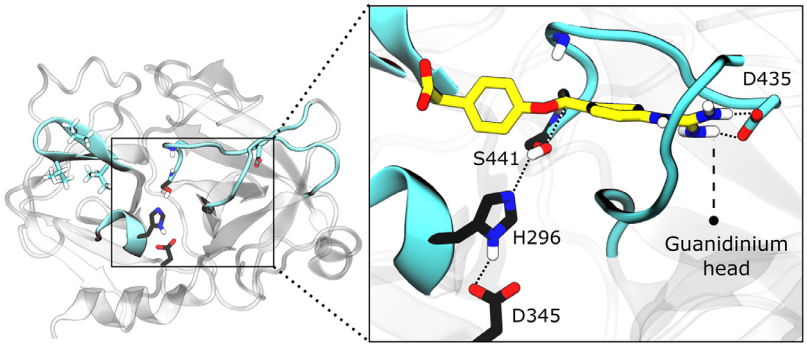

Fig. 5. TMPRSS2 protease domain and GBPA interaction. A TMPRSS2 structure model is shown in the left panel, the active site is highlighted in cyan and catalytic triad residues are shown in black. The representative structure of GBPA bound to TMPRSS2 in a reactive complex is shown in the right panel. The GBPA guanidinium head forms a salt bridge with Asp-435 inside the S1 pocket. This transient complex, which is similar for Camostat, is prone to be catalyzed at the ester bond interacting with Ser-441, leading to a covalent complex with TMPRSS2 inhibited.

The present study shows that also SARS-CoV-2 can use TTSPs other than TMPRSS2 for S protein activation. Whether the TTSPs found here to activate SARS-2-S upon directed expression play a role in viral spread in the host remains to be investigated. Expression analyses suggest that they may. TMPRSS13 activated SARS-2-S with similar efficiency as TMPRSS2 and TMPRSS13 mRNA was found to be coexpressed with ACE2 in type II pneumocytes, goblet and club cells and basal cells. Moreover, TMPRSS13 was expressed in blood cells, which may constitute a target for SARS-CoV-2 infection in some patients. Finally, and most notably, SARS-2-S activating TTSPs showed distinct expression patterns in the upper respiratory tract and several potential target cells coexpressed ACE2 jointly with a novel S protein activating TTSP but not TMPRSS2. Although viral spread supported by TMPRSS13 and potentially other SARS-2-S activating TTSPs could contribute to transmission and pathogenesis, it would still be sensitive to blockade by Camostat mesylate. Thus, usage of auxiliary TTSPs for S protein activation would not confer Camostat mesylate resistance to SARS-CoV-2.

In animals and humans Camostat mesylate is rapidly hydrolyzed into the active metabolite 4-(4-guanidinobenzoyloxy) phenylacetic acid (GBPA), which is further hydrolyzed to 4-guanidinobenzoic acid (GBA) [18–20]. GBPA was known to retain protease inhibitor activity [50,63] but it was unclear whether GBPA would block TMPRSS2 activity with the same efficiency as Camostat mesylate. Inhibition studies carried out with recombinant TMPRSS2 demonstrated that although FOY-251 robustly blocked TMPRSS2 activity, the compound was about 10-fold less active than Camostat mesylate, which roughly matches results reported for other proteases [64]. This finding raised

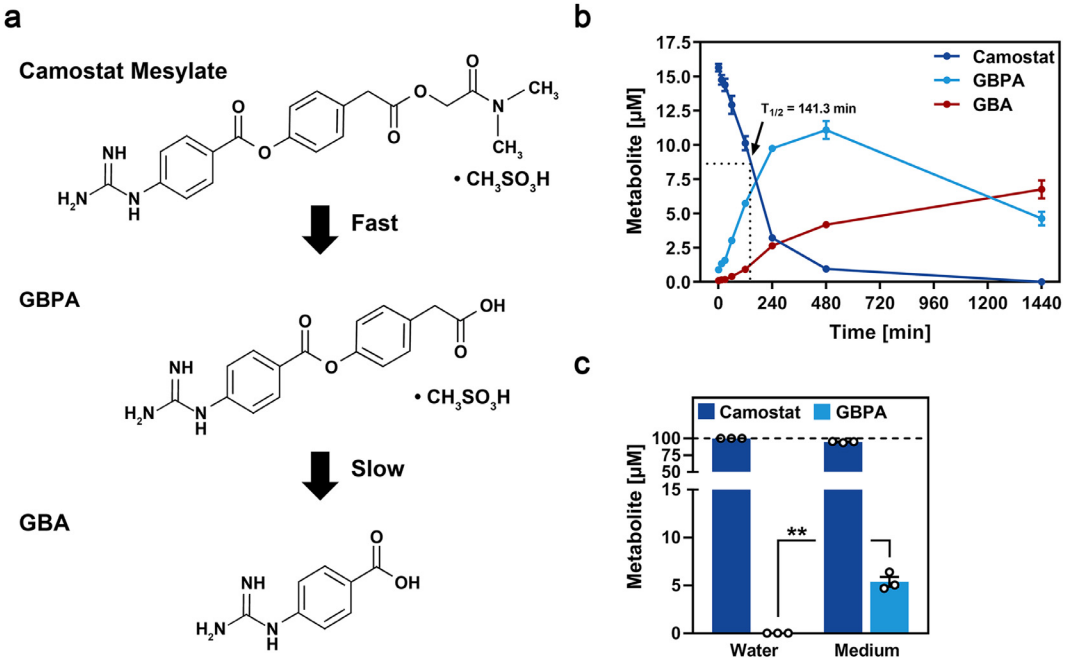

Fig. 6. Camostat mesylate is rapidly converted into GBPA in the presence of cell culture medium. (**a**) Metabolization of Camostat mesylate. (**b**) LC-MS/MS determination of Camostat, GBPA and GBA in culture medium containing FCS. Camostat mesylate was added to FCS-containing culture medium at a concentration of 15 μM. Samples were taken after incubation for 1, 15, 30, 60, 120, 240, 480, and 1,440 min at 37 °C, snap-frozen and stored at -80 °C. Samples were analyzed by LC-MS/MS and quantified regarding their content of intact Camostat mesylate and its metabolites GBPA (active) and GBA (inactive). Presented are the average (mean) data from three biological replicates (each performed with single samples). Error bars indicate the SEM. The turnover time that is required to cause metabolization of 50 % of Camostat mesylate ($T_{1/2}$) was further calculated by a non-linear regression model and was determined to be 141.3 min (95% confidence interval = 116.5 to 171.7 min). (**c**) Relative levels of Camostat mesylate and GBPA after incubation of 15 μM Camostat mesylate in either water or FCS-containing culture medium. For normalization, the combined values of Camostat mesylate and GBPA were set as 100% and the relative fractions of the compounds were calculated. Presented are the average (mean) data from three biological replicates (each performed with single samples). Error bars indicate SEM. Statistical significance of differences in GBPA levels following incubation of Camostat mesylate in either water or FCS-containing culture medium was analyzed by paired, two-tailed student's t-test (P = 0.0090). Abbreviations: FOY-51/GBPA = 4-(4-guanidinobenzoyloxy)phenylacetic acid; GBA = 4-guanidinobenzoic acid.

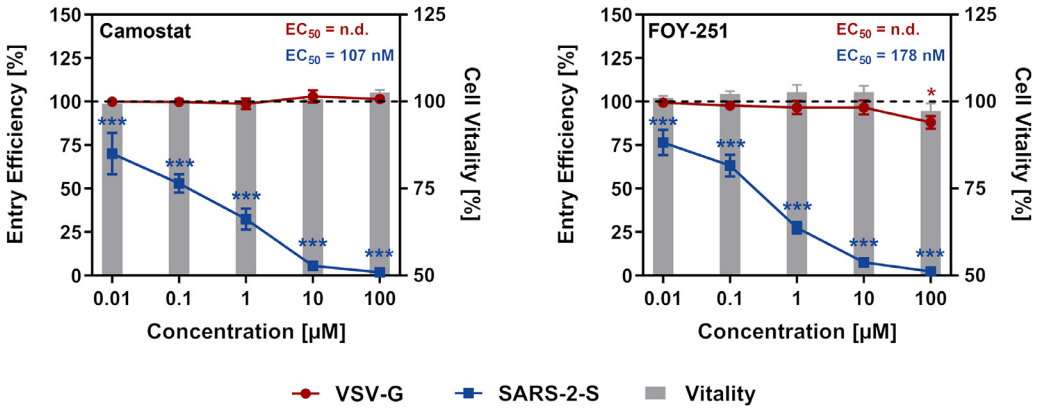

Fig. 7. Camostat mesylate and FOY-251 inhibit SARS-2-S-driven cell entry with comparable efficiency. Calu-3 cells were pre-incubated with different concentrations of Camostat mesylate (left panel), FOY-251 (right panel) or DMSO (control, indicated by dashed lines) for 2 h, before being inoculated with pseudotype particles bearing VSV-G (red) or SARS-2-S (blue). Alternatively, in order to analyze potential negative effects of Camostat mesylate and FOY-251 on cell vitality (grey bars), cells received medium instead of pseudotype particles and were further incubated. At 16 h post inoculation, pseudotype entry and cell vitality were analyzed by measuring the activity of virus-encoded luciferase in cell lysates or intracellular adenosine triphosphate levels (CellTiter-Glo assay), respectively. Data were further normalized and entry efficiency/cell vitality in the absence of Camostat mesylate and FOY-251 was set as 100%. Shown are the average (mean) data obtained from three biological replicates, each performed with four technical replicates. Error bars indicate SEM. Statistical significance of differences in entry efficiency/cell vitality in Camostat mesylate - or FOY-251-treated cells versus control-treated cells was analyzed by two-way ANOVA with Dunnett's posttest (*P* values, from left to right: Camostat/VSV-G [0.9999; 0.9999; 0.9996; 0.9733; 0.9986]; Camostat/SARS-2-S [0.0001; 0.0001; 0.0001; 0.0001; 0.0001]; Camostat/Cell vitality [0.9999; 0.9999; 0.9999; 0.9998; 0.9810]; FOY-251/VSV-G [0.9997; 0.9730; 0.8867; 0.8838; 0.0326]; FOY-251/SARS-2-S [0.0001; 0.0001; 0.0001; 0.0001; 0.0001]; FOY-251/Cell vitality [0.9986; 0.9765; 0.9455; 0.9460; 0.9612]).

the question whether Camostat mesylate conversion into GBPA also occurs in cell culture systems used to assess antiviral activity of Camostat mesylate. Indeed, Camostat mesylate was rapidly converted into GBPA in the presence of fetal calf serum similar to findings with human plasma [20]. The rapid Camostat mesylate metabolization may account for Camostat mesylate and FOY-251 exerting roughly comparable antiviral activity when cells were preincubated with these compounds for 2 h in the presence of serum. However, providing formal proof for this hypothesis will be challenging since the half-life of Camostat mesylate in human plasma is less than 1 min [20]. Nevertheless, the EC_{50} measured for FOY-251, 0.178 μM, has important implications for COVID-19 treatment, considering that continuous IV infusion of Camostat mesylate (40 mg) resulted in a maximal plasma GBPA concentration of 0.22 μM and peak plasma concentrations of GBPA in humans upon oral intake of 200 mg Camostat mesylate can reach 0.25 μM (http://www.shijiebiaopin.net/upload/product/201272318373223.PDF). Provided that concentrations in plasma and in respiratory epithelium are comparable, this would suggest that GBPA peak levels attained with the dosage approved for pancreatitis treatment (200 mg Camostat mesylate three times a day) would be sufficient to exert antiviral activity. Finally, the recently reported covalent binding of Camostat mesylate to TMPRSS2 might prolong antiviral activity [32].

Collectively, our present results indicate that Camostat mesylate constitutes a viable treatment option for COVID-19 and a recently published report indeed provided evidence that Camostat mesylate can protect from organ failure in severe COVID-19 [65].

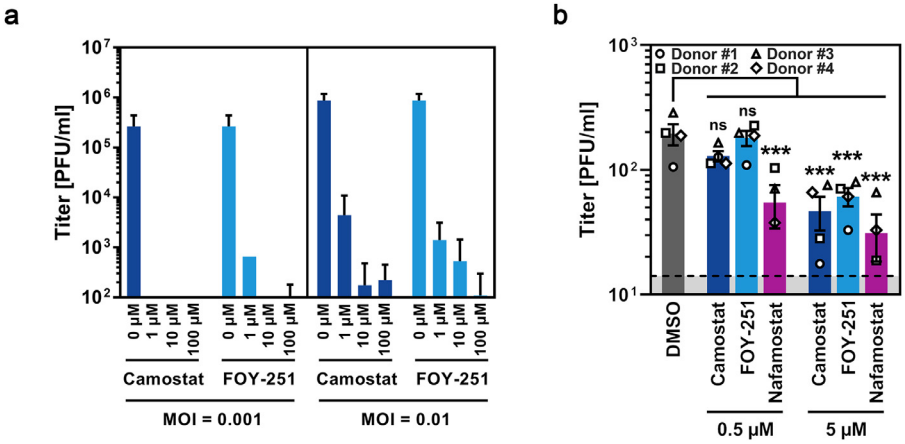

Fig. 8. Camostat mesylate and FOY-251 inhibit SARS-CoV-2 infection with comparable efficiency. (**a**) Calu-3 cells were pre-incubated for 2h with double concentration of Camostat mesylate or FOY-251 as indicated. DMSO-treated cells served as control. Thereafter, cells were infected with SARS-CoV-2. After 1 h of incubation, the inoculum was removed and cells were washed with PBS, before culture medium containing inhibitor or DMSO was added. Culture supernatants were harvested at 24 h post infection and subjected to standard plaque formation assay. Viral titers were determined as plaque forming units per ml (pfu/ml). Presented are the data from a single experiment performed with technical triplicates and the results were confirmed in a separate experiment with another SARS-CoV-2 isolate. Error bars indicate the standard deviation. (**b**) Precision-cut lung slices (PCLS) from four donors were pre-treated with 0.5 or 5 μM Camostat mesylate, FOY-251 or Nafamostat mesylate before being inoculated with SARS-CoV-2. DMSO-treated PCLS served as control. After 1 h of incubation, the inoculum was removed and PCLS were washed with PBS, before culture medium containing the respective inhibitor (or DMSO) was added. Culture supernatants were harvested at 24 h post infection and subjected to standard plaque formation assay. Presented are the data from four biological replicates, each performed with four (donor 1) or three (donor 2-4) technical replicates. Error bars indicate the SEM. One-way ANOVA with Dunnett's posttest was used for statistical analysis. *P* values, from left to right: 0.5 μM Camostat [0.1551]; 0.5 μM FOY-251 [0.9919]; 0.5 μM Nafamostat [0.0006]; 5 μM Camostat [0.0003]; 5 μM FOY-251 [0.0010]; 5 μM Nafamostat [0.0001]).

Author contributions

M.H., H.M., F.N., J.M.S., M.K. and S.P. designed the study. M.H., H. H.-W., J.C.S., N.K., P.A., L.K.S., O.S.S., J.B.H., T.H., L.R., S.O., T.Y., K.Y., and J.M.S., performed research. M.H., H.H.-W., J.C.S., H.M., N.K., T.H., F.N. J. S.M., M.K. and S.P. analyzed the data. M.W., O.D., A.B., D.J. and S.L. provided essential reagents. M.H. and S.P. wrote the manuscript. All authors revised the manuscript and read and approved the final version of the manuscript.

Data sharing statement

All data relevant for the study are shown in the manuscript or the supplementary materials. Unprocessed data will be made available upon reasonable request.

Declaration of Competing Interests

H.H-W., N.K., L.K.S., O.S.S., J.B.H., M.W., S.O., O.D., D.J., S.L., F.N., M.K. have nothing to disclose. T.Y., K.Y., H.M. report personal fees from Ono Pharmaceutical, during the conduct of the study. M.H. reports grants from Deutsche Forschungsgemeinschaft (DFG, German Research Foundation), during the conduct of the study. J.C.S. reports personal fees from Google, personal fees from Meliora Therapeutics, outside the submitted work. J.C.S. is an employee of Google. This work was performed outside of her affiliation with Google and used no proprietary knowledge or materials from Google. P.A. reports grants from Country of Lower Saxony, during the conduct of the study. T. H. reports grants from Deutsche Forschungsgemeinschaft (DFG) SFB/TRR 186, during the conduct of the study. L.R. reports grants from Bayer AG, outside the submitted work. A.B. reports grants from Fraunhofer DRECOR (Drug Repurposing for Corona), during the conduct of the study; other from Fraunhofer ITEM, outside the submitted work. J.M.S. reports grants from NIH, grants from New York Community Trust, grants from Damon Runyon Foundation, grants from American Cancer Society, grants from Department of Defense, during the conduct of the study; personal fees from Meliora Therapeutics, personal fees from Tyra Biosciences, personal fees from Ono Pharmaceutical, outside the submitted work. S.P. reports grants from Bundesministerium für Bildung und Forschung, grants from Deutsche Forschungsgemeinschaft, grants from Country of Lower Saxony, during the conduct of the study; other from Ono Pharmaceutical, outside the submitted work.

Acknowledgments

We are grateful for in-depth discussions with Katarina Elez, Tuan Le, Moritz Hoffmann (FU Berlin) and the members of the JEDI COVID-19 grand challenge. We further thank Inga Nehlmeier for excellent technical support. Research in the Sheltzer Lab was supported by NIH grants 1DP5OD021385 and R01CA237652-01, a Damon Runyon-Rachleff Innovation award, an American Cancer Society Research Scholar Grant, and a grant from the New York Community Trust. The Noé lab was supported by Deutsche Forschungsgemeinschaft DFG (SFB/TRR 186, Project A12), the European Commission (ERC CoG 772230 "ScaleCell"), the Berlin Mathematics center MATH+ (AA1-6) and the federal ministry of education and research BMBF (BIFOLD). The Pöhlmann lab was supported by the Bundesministerium für Bildung und Forschung (RAPID Consortium, 01KI1723D; RENACO consortium, 01KI20328A; SARS_S1S2, 01KI20396), Deutsche Forschungsgemeinschaft (PO 716/11-1) and the Country of Lower Saxony. The Kjolby lab was supported by the Lundbeck Foundation (M.K., O.S.) and the Novo Nordisk Foundation (M.K.). The work in the Braun lab was partly funded by the Fraunhofer Internal Programs under Grant No. Anti-Corona 840260 DRECOR (Drug Repurposing for Corona).

Supplementary materials

Supplementary material associated with this article can be found in the online version at doi:10.1016/j.ebiom.2021.103255.

References

[1] World Health Organization (WHO). Coronavirus disease (COVID-19). Situation Report 2020;184.
[2] Santos J, Brierley S, Gandhi MJ, Cohen MA, Moschella PC, Declan ABL. Repurposing therapeutics for potential treatment of SARS-CoV-2: a review. Viruses 2020;12(7).
[3] Beigel JH, Tomashek KM, Dodd LE, et al. Remdesivir for the treatment of COVID-19 - preliminary report. N Engl J Med 2020.
[4] Wang Y, Zhang D, Du G, et al. Remdesivir in adults with severe COVID-19: a randomised, double-blind, placebo-controlled, multicentre trial. Lancet 2020;395 (10236):1569–78.
[5] Hoffmann M, Kleine-Weber H, Schroeder S, et al. SARS-CoV-2 cell entry depends on ACE2 and TMPRSS2 and is blocked by a clinically proven protease inhibitor. Cell. 2020;181(2):271–80 e8.
[6] Kawase M, Shirato K, van der Hoek L, Taguchi F, Matsuyama S. Simultaneous treatment of human bronchial epithelial cells with serine and cysteine protease inhibitors prevents severe acute respiratory syndrome coronavirus entry. J Virol 2012;86(12):6537–45.
[7] Abe M. Use of FOY-305 for the treatment of pain attacks associated with chronic pancreatitis. New Horiz Med 1980;12:233.
[8] Ishii K. Evaluation of the efficacy of FOY-305 in pancreatitis: multicenter, double-blind study. New Horiz Med 1980;12:261.
[9] Ohshio G, Saluja AK, Leli U, Sengupta A, Steer ML. Esterase inhibitors prevent lysosomal enzyme redistribution in two noninvasive models of experimental pancreatitis. Gastroenterology 1989;96(3):853–9.
[10] Iwata-Yoshikawa N, Okamura T, Shimizu Y, Hasegawa H, Takeda M, Nagata N. TMPRSS2 contributes to virus spread and immunopathology in the airways of murine models after coronavirus infection. J Virol 2019;93(6).
[11] Zhou Y, Vedantham P, Lu K, et al. Protease inhibitors targeting coronavirus and filovirus entry. Antiviral Res 2015;116:76–84.
[12] Gierer S, Bertram S, Kaup F, et al. The spike protein of the emerging betacoronavirus EMC uses a novel coronavirus receptor for entry, can be activated by TMPRSS2, and is targeted by neutralizing antibodies. J Virol 2013;87(10): 5502–11.
[13] Qian Z, Dominguez SR, Holmes KV. Role of the spike glycoprotein of human Middle East respiratory syndrome coronavirus (MERS-CoV) in virus entry and syncytia formation. PLoS One 2013;8(10):e76469.
[14] Shirato K, Kawase M, Matsuyama S. Middle East respiratory syndrome coronavirus infection mediated by the transmembrane serine protease TMPRSS2. J Virol 2013;87(23):12552–61.
[15] Simmons G, Gosalia DN, Rennekamp AJ, Reeves JD, Diamond SL, Bates P. Inhibitors of cathepsin L prevent severe acute respiratory syndrome coronavirus entry. Proc Natl Acad Sci U S A. 2005;102(33):11876–81.
[16] Park JE, Li K, Barlan A, et al. Proteolytic processing of Middle East respiratory syndrome coronavirus spikes expands virus tropism. Proc Natl Acad Sci U S A. 2016;113(43):12262–7.
[17] Puelles VG, Lutgehetmann M, Lindenmeyer MT, et al. Multiorgan and Renal Tropism of SARS-CoV-2. N Engl J Med 2020.
[18] Beckh K, Goke B, Muller R, Arnold R. Elimination of the low-molecular weight proteinase inhibitor camostate (FOY 305) and its degradation products by the rat liver. Res Exp Med (Berl) 1987;187(6):401–6.
[19] Beckh K, Weidenbach H, Weidenbach F, Muller R, Adler G. Hepatic and pancreatic metabolism and biliary excretion of the protease inhibitor camostat mesilate. Int J Pancreatol 1991;10(3-4):197–205.
[20] Midgley I, Hood AJ, Proctor P, et al. Metabolic fate of 14C-camostat mesylate in man, rat and dog after intravenous administration. Xenobiotica 1994;24(1):79–92.
[21] Brinkmann C, Hoffmann M, Lubke A, et al. The glycoprotein of vesicular stomatitis virus promotes release of virus-like particles from tetherin-positive cells. PLoS One 2017;12(12):e0189073.
[22] Chaipan C, Kobasa D, Bertram S, et al. Proteolytic activation of the 1918 influenza virus hemagglutinin. J Virol 2009;83(7):3200–11.
[23] Jung H, Lee KP, Park SJ, et al. TMPRSS4 promotes invasion, migration and metastasis of human tumor cells by facilitating an epithelial-mesenchymal transition. Oncogene 2008;27(18):2635–47.
[24] Bertram S, Glowacka I, Muller MA, et al. Cleavage and activation of the severe acute respiratory syndrome coronavirus spike protein by human airway trypsin-like protease. J Virol 2011;85(24):13363–72.
[25] Zmora P, Hoffmann M, Kollmus H, et al. TMPRSS11A activates the influenza A virus hemagglutinin and the MERS coronavirus spike protein and is insensitive against blockade by HAI-1. J Biol Chem 2018;293(36):13863–73.
[26] Zmora P, Blazejewska P, Moldenhauer AS, et al. DESC1 and MSPL activate influenza A viruses and emerging coronaviruses for host cell entry. J Virol 2014;88 (20):12087–97.
[27] Hoffmann M, Müller MA, Drexler JF, et al. Differential sensitivity of bat cells to infection by enveloped RNA viruses: coronaviruses, paramyxoviruses, filoviruses, and influenza viruses. PLoS One 2013;8(8):e72942.

[28] Hoffmann M, Kleine-Weber H, Pohlmann S. A multibasic cleavage site in the spike protein of SARS-CoV-2 is essential for infection of human lung cells. Mol Cell 2020;78(4):779–84 e5.
[29] Berger Rentsch M, Zimmer G. A vesicular stomatitis virus replicon-based bioassay for the rapid and sensitive determination of multi-species type I interferon. PLoS One 2011;6(10):e25858.
[30] Stefano R, Russ BA, Tianyun L, et al. Homology Modeling of TMPRSS2 Yields Candidate Drugs That May Inhibit Entry of SARS-CoV-2 into Human Cells 2020.
[31] Prinz JH, Wu H, Sarich M, et al. Markov models of molecular kinetics: generation and validation. J Chem Phys 2011;134(17):174105.
[32] Hempel T, Raich L, Olsson S, et al. Molecular mechanism of inhibiting the SARS-CoV-2 cell entry facilitator TMPRSS2 with camostat and nafamostat. Chemical Science 2021.
[33] Neuhaus V, Danov O, Konzok S, et al. Assessment of the cytotoxic and immunomodulatory effects of substances in human precision-cut lung slices. J Vis Exp 2018(135).
[34] Consortium GT. The genotype-tissue expression (GTEx) project. Nat Genet 2013;45(6):580–5.
[35] Smith JC, Sausville EL, Girish V, et al. Cigarette smoke exposure and inflammatory signaling increase the expression of the SARS-CoV-2 receptor ACE2 in the respiratory tract. Dev Cell 2020;53(5):514–29 e3.
[36] Ulyanov D. DmitryUlyanov/Multicore-TSNE 2020. https://github.com/DmitryUlyanov/Multicore-TSNE.
[37] Wolf FA, Angerer P, Theis FJ. SCANPY: large-scale single-cell gene expression data analysis. Genome Biol 2018;19(1):15.
[38] Ardini-Poleske ME, Clark RF, Ansong C, et al. LungMAP: the molecular atlas of lung development program. Am J Physiol Lung Cell Mol Physiol 2017;313(5):L733–L40.
[39] Muus C, Luecken MD, Eraslan G, et al. Integrated analyses of single-cell atlases reveal age, gender, and smoking status associations with cell type-specific expression of mediators of SARS-CoV-2 viral entry and highlights inflammatory programs in putative target cells. bioRxiv. 2020:2020.04.19.049254.
[40] Cuzick J, Boyle P. Trends in cervix cancer mortality. Cancer Surv 1988;7(3):417–39.
[41] Travaglini KJ, Nabhan AN, Penland L, et al. A molecular cell atlas of the human lung from single-cell RNA sequencing. Nature 2020;587(7835):619–25.
[42] Reyfman PA, Walter JM, Joshi N, et al. Single-Cell transcriptomic analysis of human lung provides insights into the pathobiology of pulmonary fibrosis. Am J Respir Crit Care Med 2019;199(12):1517–36.
[43] Deprez M, Zaragosi LE, Truchi M, et al. A single-cell atlas of the human healthy airways. Am J Respir Crit Care Med 2020.
[44] Ding Y, He L, Zhang Q, et al. Organ distribution of severe acute respiratory syndrome (SARS) associated coronavirus (SARS-CoV) in SARS patients: implications for pathogenesis and virus transmission pathways. J Pathol 2004;203(2):622–30.
[45] Hamming I, Timens W, Bulthuis ML, Lely AT, Navis G, van Goor H. Tissue distribution of ACE2 protein, the functional receptor for SARS coronavirus. A first step in understanding SARS pathogenesis. J Pathol 2004;203(2):631–7.
[46] Lukassen S, Chua RL, Trefzer T, et al. SARS-CoV-2 receptor ACE2 and TMPRSS2 are primarily expressed in bronchial transient secretory cells. EMBO J 2020;39(10):e105114.
[47] Sungnak W, Huang N, Becavin C, et al. SARS-CoV-2 entry factors are highly expressed in nasal epithelial cells together with innate immune genes. Nat Med 2020;26(5):681–7.
[48] Ziegler CGK, Allon SJ, Nyquist SK, et al. SARS-CoV-2 receptor ACE2 is an interferon- stimulated gene in human airway epithelial cells and is detected in specific cell subsets across tissues. Cell. 2020;181(5):1016–35 e19.
[49] Carithers LJ, Moore HM. The genotype-tissue expression (GTEx) project. Biopreserv Biobank 2015;13(5):307–8.
[50] Ohki S, Nishiyama H, Ozeki K, Ito H, Hirata F. Studies on absorption, distribution, metabolism and excretion of [14C] FOY-305. Gendai-Iryo 1980;12:71–82.
[51] Group RC, Horby P, Lim WS, et al. Dexamethasone in hospitalized patients with COVID- 19 - preliminary report. N Engl J Med 2020.
[52] Breining P, Frolund AL, Hojen JF, et al. Camostat mesylate against SARS-CoV-2 and COVID-19-rationale, dosing and safety. Basic Clin Pharmacol Toxicol 2020.
[53] Hatesuer B, Bertram S, Mehnert N, et al. Tmprss2 is essential for influenza H1N1 virus pathogenesis in mice. PLoS Pathog 2013;9(12):e1003774.
[54] Sakai K, Ami Y, Tahara M, et al. The host protease TMPRSS2 plays a major role in in vivo replication of emerging H7N9 and seasonal influenza viruses. J Virol 2014;88(10):5608–16.
[55] Tarnow C, Engels G, Arendt A, et al. TMPRSS2 is a host factor that is essential for pneumotropism and pathogenicity of H7N9 influenza A virus in mice. J Virol 2014;88(9):4744–51.
[56] Böttcher E, Matrosovich T, Beyerle M, Klenk HD, Garten W, Matrosovich M. Proteolytic activation of influenza viruses by serine proteases TMPRSS2 and HAT from human airway epithelium. J Virol 2006;80(19):9896–8.
[57] Sakai K, Sekizuka T, Ami Y, et al. A mutant H3N2 influenza virus uses an alternative activation mechanism in TMPRSS2 knockout mice by loss of an oligosaccharide in the hemagglutinin stalk region. J Virol 2015;89(9):5154–8.
[58] Kuhn N, Bergmann S, Kosterke N, et al. The proteolytic activation of (H3N2) influenza a virus hemagglutinin is facilitated by different type II transmembrane serine proteases. J Virol 2016;90(9):4298–307.
[59] Harbig A, Mernberger M, Bittel L, et al. Transcriptome profiling and protease inhibition experiments identify proteases that activate H3N2 influenza A and influenza B viruses in murine airway. J Biol Chem 2020.
[60] Laporte M, Stevaert A, Raeymaekers V, et al. Hemagglutinin cleavability, acid stability, and temperature dependence optimize influenza B virus for replication in human airways. J Virol 2019;94(1).
[61] Limburg H, Harbig A, Bestle D, et al. TMPRSS2 is the major activating protease of influenza a virus in primary human airway cells and influenza b virus in human type II pneumocytes. J Virol 2019;93(21).
[62] Sakai K, Ami Y, Nakajima N, et al. TMPRSS2 independency for haemagglutinin cleavage in vivo differentiates influenza b virus from influenza A. Virus. Sci Rep. 2016;6:29430.
[63] Yonezawa H. Discrepancy between the potency of various trypsin inhibitors to inhibit trypsin activity and the potency to release biologically active cholecystokinin- pancreozymin. Jpn J Physiol 1984;34(5):849–56.
[64] Senokuchi K, Nakai H, Nakayama Y, et al. New orally active serine protease inhibitors. J Med Chem 1995;38(14):2521–3.
[65] Hofmann-Winkler H, Moerer O, Alt-Epping S, et al. Camostat mesylate may reduce severity of coronavirus disease 2019 sepsis: a first observation. Crit Care Explor 2020;2(11):e0284.